Journal of Magnetism and Magnetic Materials 471 (2019) 549–554

Contents lists available at ScienceDirect

Journal of Magnetism and Magnetic Materials

journal homepage: www.elsevier.com/locate/jmmm

Research articles

Magnetic and structural changes in $Cu_{1-x}Al_x$ alloy matrix – Embedded Fe nanoparticle systems

M.S. Kurt[a,b,*], S.H. Baker[a], M. Roy[a], M.R. Lees[c]

[a] Department of Physics and Astronomy, University of Leicester, Leicester LE1 7RH, UK
[b] Department of Fundemantal Science, Erzurum Technical University, Erzurum, Turkey
[c] Department of Physics, The University of Warwick, Coventry CV4 7AL, UK

ARTICLE INFO

Keywords:
Fe nanoparticles
Magnetic
Atomic structure
EXAFS

ABSTRACT

We describe the atomic structure and magnetism in Fe nanoparticles (~2 nm) ebedded in a $Cu_{1-x}Al_x$ alloy matrix. Nanocomposite films for these studies were prepared directly from gas phase using a flexible co-deposition technique under Ultra-High Vacuum (UHV) conditions. Fe nanoparticles and the alloy matrix were prepared using a gas aggregation source and MBE sources respectively. Extended x-ray absorption fine structure (EXAFS) experiments indicate that the embedded Fe nanoparticles retain a bcc structure for Al-contents greater than $x = 0.13$ but, for Al-contents lower than this value, Fe nanoparticles have both fcc and bcc structures. The magnetic moment per Fe atom initially increases with increasing Al-content due to the bcc structure becoming more dominant in the embedded nanoparticles as the Al-content is increased, but then decreases with further increase in Al-content. This decrease is consistent with a modest degree of alloying between Fe and Al atoms at the particle/matrix interfaces.

1. Introduction

Novel magnetic properties are displayed by metal particles at nanosizes (with size in the range 1–10 nm), compared to the corresponding macroscopic material, due to the location of under-coordinated atoms at the particle surface. Even very small changes in d and f energy bands can cause significant alterations in the magnetic properties of transition metals and rare earth metals respectively, and this leads to nanoparticle properties that are size-dependent [1–3]. Performing Stern-Gerlach experiments on cluster beams of transition metals such as Fe, Co and Ni revealed that enhancement of atomic magnetic moments, relative to corresponding bulk form of the respective materials, could be observed [1,2]. Thereafter, the enhancement of atomic moments was also confirmed in Fe nanoparticles on a substrate using x-ray magnetic circular dichroism (XMCD) experiments [4–6].

Atomic structure of nanoparticles can be changed by depositing them in an appropriate matrix of a different material. Atomic structure plays a highly critical role in determining the magnetic properties of materials, as has been seen in studies of Fe and Co nanoparticles in various matrices [7–19]. In many of these studies, the low energy cluster beam deposition (LECBD) technique [20] was used to prepare the nanocomposite samples. This is due to the high degree of control and flexbility afforded by the technique during the production of granular materials, in which gas phase nanoparticles and matrix materials are deposited onto a surface simultaneously from a nanoparticle source and molecular beam epitaxy (MBE) sources respectively.

Previous reports show that embedding Fe and Co nanoparticles in different matrix materials leads to changes in the atomic structure, depending on the host matrix materials [7–18], as mentioned above. [These studies show that changes in the nanoparticle structure occur “pseudoepitaxially” due to the embedding matrix rather than to thin film effects]. For instance, after embedding Co nanoparticles in an Fe matrix, the structure of the Co nanoparticles switches from hcp (as in bulk Co) to the same structure (bcc) of the Fe host matrix [14]. After embedding Fe nanoparticles in a Cu matrix, the bulk bcc atomic structure of Fe switches to the same fcc structure of the host Cu matrix [16,17]. Given that the lattice parameters of Cu and the high temperature fcc phase of bulk Fe (above 1200 K) are 3.61 Å and 3.59 Å respectively, this “pseudo-epitaxially” driven change in structure of the Cu embedded Fe nanoparticles is not surprising. In previous studies, we have shown that the atomic magnetic moment in Cu-embedded fcc Fe nanoparticles is significantly less than the bulk Fe value (0.4–0.9 μ_B/atom versus 2.2 μ_B/atom) [17].

The possibility of forming the f.c.c. structure in Fe at room temperature has attracted much interest, in part due to the many

* Corresponding author at: Department of Fundemantal Science, Erzurum Technical University, Erzurum, Turkey.
E-mail address: mustafa.kurt@erzurum.edu.tr (M.S. Kurt).

https://doi.org/10.1016/j.jmmm.2018.08.040
Received 3 May 2018; Received in revised form 7 August 2018; Accepted 15 August 2018
Available online 23 August 2018
0304-8853/

calculations carried out previously for bulk f.c.c. Fe [21–23]. These works indicate the possibility of enhanced atomic moments in fcc Fe, to values as high as 2.5 μ_B/atom (i.e. higher than in bcc Fe). Moreover, the calculations show that there is a strong dependence of atomic moment on the fcc lattice parameter, with a transition from a low spin to a high spin state as the lattice parameter is increased in the range 3.4–3.7 Å. This prompted studies of ultra-thin fcc Fe films grown epitaxially on $Cu_{1-x}Au_x$ substrates [24,25], since $Cu_{1-x}Au_x$ has an fcc structure with a lattice parameter which increases with increasing Au content. The Fe atomic moments were found to increase as the lattice parameter of the substrate increased. Subsequently, we have also shown that embedding Fe nanopaticles in a $Cu_{1-x}Au_x$ alloy matrix leads to a stretch in both the fcc matrix structure and the embedded fcc Fe nanoparticles with increasing Au-content [19]. [In fact the embedded Fe nanoparticles were found to expand tetragonally rather than isotropically in an fcc structure]. Consistent with theory [17,21–23], as a result of this stretch the atomic moments of Fe were increased sharply to values around 2.5 ± 0.3 μ_B/atom [19]. Managing embedded nanoparticle and matrix material structures at the atomic scale in this way provides a high level of control over the magnetic properties of nanocomposite materials. It can play an important role in the imrovement of 'new' cluster-assembled magnetic materials in number of areas, such as high density data storage [26] and various biomedical applications [27,28].

Similarly to $Cu_{1-x}Au_x$, the alloy $Cu_{1-x}Al_x$ also has an fcc structure with a lattice parameter which increases with increasing Al content. The purpose of the work presented here was to investigate whether Fe nanoparticles embedded in $Cu_{1-x}Al_x$ also show significant moment ehancements due to structure stretch (as measured for those embedded in $Cu_{1-x}Au_x$). Hence we present details of the measurements of atomic structure and magnetism in ferromagnetic Fe nanoparticles embedded in a $Cu_{1-x}Al_x$ alloy matrix. The nanocomposite films were prepared in the form of thin films using a flexible LECBD technique [20], therefore providing a high-level of control over the nanostructure of the samples. The results indicate that the atomic structure of Fe nanoparticles have both bcc and fcc structures without any stretch in Fe-Fe interatomic distances, while Cu-Cu interatomic distances increase as the Al-content is increased in the alloy matrix. The atomic moments in the Fe nanoparticles initially increase sharply with increasing Al-content to close to the bulk bcc value (2.2 μ_B/atom), then decrease slightly which is consistent with some alloying between Fe and Al atoms with increasing Al-content in the alloy matrix. EXAFS experiments were used to determine the atomic structure in both Fe nanoparticles and alloy matrix, whereas magnetism in the nanocomposite films was measured using VSM and SQUID magnetometry.

2. Experimental details

Samples of Fe nanoparticles embedded in $Cu_{1-x}Al_x$ alloy matrix were prepared in thin film form using a co-deposition technique under ultra-high-vacuum (UHV) conditions. A gas aggregation nanoparticle source was used to produce the Fe nanoparticles, while Cu and Al were produced using molecular beam epitaxy (MBE) sources. Detailed information about the nanoparticle source is given elsewhere [29,30]. Briefly, Fe nanoparticles are produced by nanoparticle source direct from gas phase, with a log-normal distribution (diameters) in the 1–5 nm range with a strong peak at around 2 nm. The size of nanoparticles was monitored using a quadrupole filter. A quartz crystal thickness monitor (XTM) was used to control deposition rates of embedded nanoparticles and matrix materials. In order to isolate effectively the Fe nanoparticles from one another, and hence avoid particle-particle interactions, the Fe nanoparticle volume fraction in the films was around 5% in all cases. [5% volume fraction is considerably below the 3-D percolation threshold of 24.88% [31], for which a continuous connectivity between the embedded nanoparticles and hence inter-particle effects would be expected. Previous work on embedded Fe nanoparticles, in Cu for example [17], has shown that they behave as isolated particles at a volume fraction of 5%]. The Al-content in the alloy matrix was changed from $x = 0$ to 0.31 by controlling deposition rates of Cu and Al. The nanocomposite films were deposited onto Si (1 0 0) substrate for magnetometry and EXAFS measurements. To protect the nanocomposite films from oxidation after removing from the ultra-high vacuum deposition chamber, and from any unwanted effects from the substrate, a capping layer of Ag, about 500 Å, and a buffer layer of Ag, about 250 Å, were deposited for each sample respectively. For comparison purposes, a pure Fe film was prepared using an MBE source.

Fe K edge and Cu K edge EXAFS experiments were carried out to investigate atomic structure in the Fe nanoparticles and the $Cu_{1-x}Al_x$ alloy matrix. These experiments were performed on beamline B18 at the Diamond Light Source. X-ray absorption spectra were obtained in fluorescence, using a 36-element Ge detector, at room temperature. The energy of the x-rays was chosen using a double crystal Si(1 1 1) monochromator, while the incident x-ray intensity was measured using an ionisation chamber which contained He gas. The EXAFS spectra $\chi(k)$ were extracted from the measured absorption spectra using the computer program PySpline [32], which enables subtraction of the background and then normalisation of the resulting spectra. Structural parameters like interatomic distances r_i, mean square variations in interatomic distance σ_i^2 (Debye–Waller factors) and coordinations N_i could be obtained by analysing these spectra. The EXAFS spectra $\chi(k)$ were analysed by using the EXCURV98 program [33] in which fast curve wave theory [34] is used to model the electron waves. Hedin–Lundqvist potentials were used in the program to calculate phase shifts and atomic scattering potentials, which account for the reduction effects on amplitude in EXAFS [35]. All errors are within the ± 2 standard deviation range limits.

A Quantum Design SQUID magnetometer and Oxford Instrument VSM magnetometer were used to investigate magnetism in the nanocomposite films. Magnetisation curves (magnetic moment versus applied magnetic field) were obtained for magnetic fields between ± 5 T at 2 K. Knowing the total amount of Fe in the nanocomposite films, and using the samples' magnetic moment saturation values, the net atomic moment per Fe atom could be measured.

3. Results and discussion

3.1. EXAFS

3.1.1. Cu K edge

Fig. 1 shows the k^3-weighted Cu K edge EXAFS spectra $k^3\chi$, and their associated Fourier transforms for samples of Fe nanoparticles embedded in matrices of (i) pure Cu (ii) $Cu_{0.92}Al_{0.08}$ (iii) $Cu_{0.87}Al_{0.13}$ (iv) $Cu_{0.82}Al_{0.18}$ respectively. Initial observation of the data for these samples shows that all four spectra look similar to each other. Pure Cu is, of course, known to have an fcc structure. It was indeed possible to obtain 4-shell fits as expected for the fcc structure for all Cu edge spectra in Fig. 1. A common method was followed when performing the fitting procedure; the values of N_i were fixed at values expected for the fcc structure, whereas r_i and σ_i^2 were allowed to vary freely. As can be expected for fcc structure, multiple scattering between the first and fourth shells was incorporated in the fit. The fit values measured are shown in Table 1, as can be seen from the results the r_i values are similar to those in fcc Cu.

The first point to note is that interatomic distances obtained for the pure Cu matrix (for the 5.8 %VFF Fe/Cu film) are consistent with the known interatomic distances in fcc Cu. It can be observed from the structural parameters in the table that Cu-Cu interatomic distances slightly stretch, while the face centred structure in the $Cu_{1-x}Al_x$ matrix is maintained, as the Al-content in the alloy matrix is increased. This is similar to the stretch in Cu-Cu interatomic distances measured in $Cu_{1-x}Au_x$, in a previous study of Fe nanoparticles embedded in $Cu_{1-x}Au_x$ [19]. It is also worth mentioning that, with increasing Al-

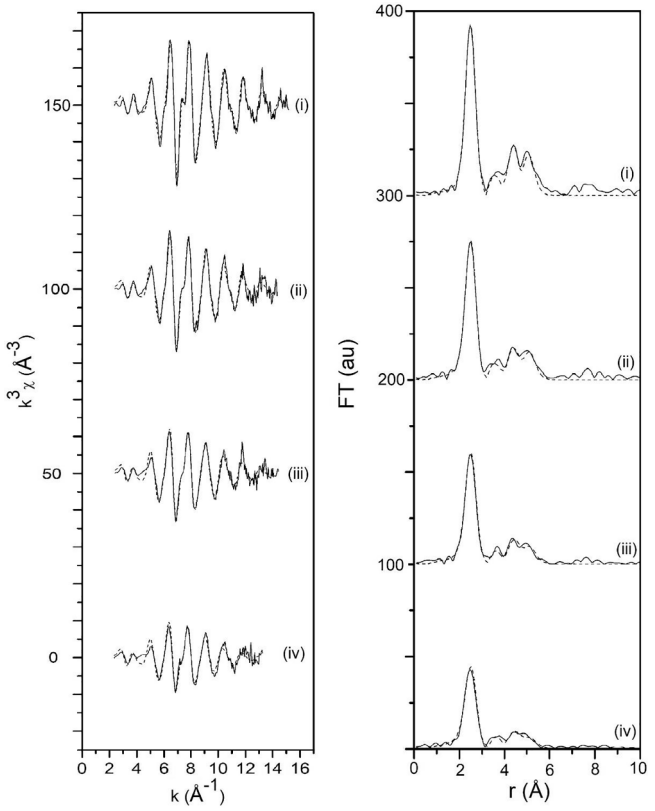

Fig. 1. Cu K edge EXAFS spectra χ, weighted by k^3, and associated Fourier transforms measured for (i) a film of Fe nanoparticles embedded in pure Cu, (ii) a film of Fe nanoparticles embedded in $Cu_{0.92}Al_{0.08}$, (iii) a film of Fe nanoparticles embedded in $Cu_{0.87}Al_{0.13}$, (iv) a film of Fe nanoparticles embedded in $Cu_{0.82}Al_{0.18}$. The full line represents the data and Fourier transform of the data while the dashed line represents the fit to the data and Fourier transform of the fit.

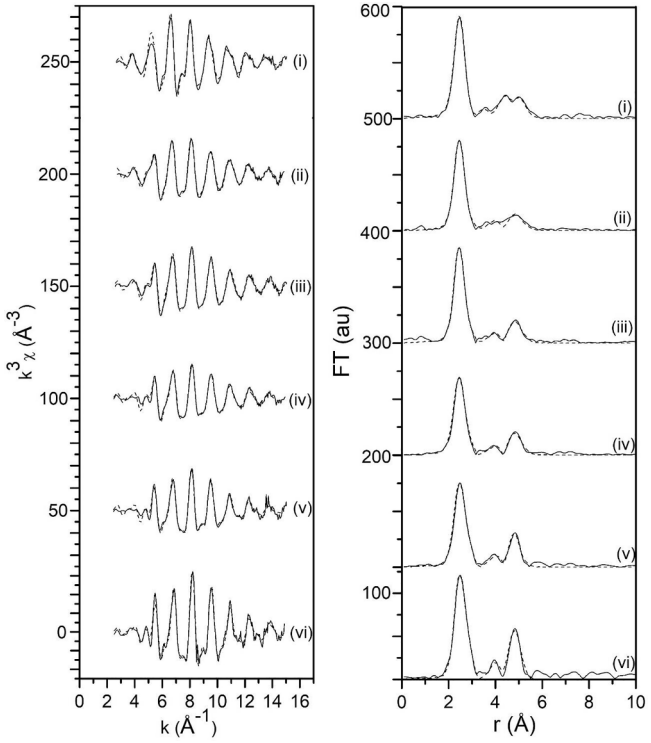

Fig. 2. Fe K edge EXAFS spectra χ, weighted by k^3, and associated Fourier transforms measured for (i) a film of Fe nanoparticles embedded in pure Cu, (ii) a film of Fe nanoparticles embedded in $Cu_{0.92}Al_{0.08}$, (iii) a film of Fe nanoparticles embedded in $Cu_{0.87}Al_{0.13}$, (iv) a film of Fe nanoparticles embedded in $Cu_{0.82}Al_{0.18}$, (v) a film of Fe nanoparticles embedded in $Cu_{0.69}Al_{0.31}$, (vi) an Fe MBE film. The full line represents the data and Fourier transform of the data while the dashed line represents the fit to the data and Fourier transform of the fit.

content in the alloy matrix, the steady increase in Debye-Waller factor indicates an increase in structural disorder.

3.1.2. Fe K edge

Fig. 2 Illustrate the k^3-weighted Fe K edge EXAFS spectra $k^3\chi$, and their associated Fourier transforms, measured for samples consisting of Fe nanoparticles embedded in matrices of (i) pure Cu (ii) $Cu_{0.92}Al_{0.08}$ (iii) $Cu_{0.87}Al_{0.13}$ (iv) $Cu_{0.82}Al_{0.18}$ (v) $Cu_{0.69}Al_{0.31}$. Also for comparison purposes, the spectrum for a pure Fe MBE film (vi) is given in the figure. It can be noted that no evidence of oxidation was apparent in any of the spectra for the embedded Fe nanoparticles. It is known from a previous study [15] (where some oxidation was allowed deliberately by using a porous C_{60} capping layer) that partial oxidation in Fe nanoparticles can cause considerable changes in the spectra of the Fe K edge EXAFS; such changes were not seen in any spectra of this study, confirming that the 500 Å Ag capping layer used here was sufficient to prevent oxidation.

From initial investigation of the Fe K edge spectrum and Fourier transform for Fe nanoparticles embedded in Cu, which is shown in Fig. 2(i), it is clear that they are similar to the corresponding data for pure Cu (see Fig. 1(i)). The analysis of the Fe edge spectrum shows that a good four shell fit is obtained for this sample which is consistent with fcc, and shows that Fe clusters have an fcc structure in pure Cu. The fit parameters r_i and $2\sigma_i^2$ are shown in Table 2, with the known fcc Fe interatomic distances. This is consistent with a previous study of Cu-embedded Fe nanoparticles [17].

As the Al content in the matrix is increased, it can be seen from Fig. 2 that the Fe K edge spectra and Fourier transforms become more like the spectrum and Fourier transform for the Fe MBE film (see Fig. 2(vi)). Analysis of the Fe MBE film spectrum shows that a good five shell fit was obtained, and the structure is bcc as expected for bulk Fe and for this sample (Multiple scattering was included between shells 1 and 5). During the fitting procedure N_i were held fixed at values for the bcc structure. Table 2 shows the obtained fit parameters, and also the known interatomic distances in bcc Fe. When Al is introduced into the Cu matrix, it is in fact not possible to obtain satisfactory fcc fits to the Fe edge spectra. However, it is possible to obtain bcc fits to the Fe edge spectra. The fit parameters obtained can be seen in Table 2.

For Fe nanoparticles in $Cu_{0.82}Al_{0.18}$ and $Cu_{0.69}Al_{0.31}$ matrices, good bcc fits to the Fe edge data were obtained. However, as can be seen from Fig. 2, for Fe nanoparticles in the $Cu_{0.92}Al_{0.08}$ and $Cu_{0.87}Al_{0.13}$ alloy matrices, the bcc fits to the Fe edge spectra were less good. One reason for this could be that there are Fe nanoparticles with both bcc and fcc structures in these samples. In an attempt to account for this in the fits, a multi-shell fit was applied to the data, with shells from both fcc and bcc structures. The values of coordinations N_i were fixed with a 50% bcc–50% fcc mixture. So the first coordination shells in the bcc and fcc structures were held at 4 and 6 (rather than 8 and 12). The second coordination shells for the bcc and fcc structures were held at 3 and 3 respectively (rather than 6 and 6), and so on. The values of r_i and $2\sigma_i^2$ were allowed to change freely in the fits. Table 3 shows the obtained fit parameters. Fig. 3 shows the modified fits to the data for these samples, and the measured data. The 50% bcc–50% fcc fits are improved relative to the bcc fits. These results indicate that Fe nanoparticles in a $Cu_{0.92}Al_{0.08}$ and $Cu_{0.87}Al_{0.13}$ alloy matrix can exist with both bcc and fcc structures. However with increasing Al-content in the matrix, the embedded Fe nanoparticles' atomic structure changes predominantly to bcc. These results differ from a previous study of Fe nanoparticles embedded in a $Cu_{1-x}Au_x$ matrix [19]. Here, the basic fcc structure of

Table 1
Structural parameters r_i and $2\sigma_i^2$ (interatomic distances and Debye–Waller factors respectively) obtained from fits to the Cu K edge EXAFS spectra measured for films of Fe nanoparticles embedded in a $Cu_{1-x}Al_x$ matrix. Also included the interatomic distances and coordinations in bulk fcc Cu.

	Shell 1	Shell 2	Shell 3	Shell 4
fcc Cu	$r_1 = 2.55$ Å	$r_2 = 3.61$ Å	$r_3 = 4.42$ Å	$r_4 = 5.11$ Å
	$N_1 = 12$	$N_2 = 6$	$N_3 = 24$	$N_4 = 12$
5.8% VFF Fe Clusters in Cu Matrix	$r_1 = 2.54 \pm 0.01$ Å	$r_2 = 3.58 \pm 0.02$ Å	$r_3 = 4.44 \pm 0.02$ Å	$r_4 = 5.11 \pm 0.01$ Å
	$2\sigma_1^2 = 0.016 \pm 0.001$ Å^2	$2\sigma_2^2 = 0.025 \pm 0.004$ Å^2	$2\sigma_3^2 = 0.023 \pm 0.001$ Å^2	$2\sigma_4^2 = 0.022 \pm 0.001$ Å^2
6.8% VFF Fe Clusters in $Cu_{0.92}Al_{0.08}$Alloy Matrix	$r_1 = 2.55 \pm 0.01$ Å	$r_2 = 3.58 \pm 0.02$ Å	$r_3 = 4.47 \pm 0.02$ Å	$r_4 = 5.15 \pm 0.02$ Å
	$2\sigma_1^2 = 0.018 \pm 0.001$ Å^2	$2\sigma_2^2 = 0.029 \pm 0.005$ Å^2	$2\sigma_3^2 = 0.030 \pm 0.003$ Å^2	$2\sigma_4^2 = 0.027 \pm 0.002$ Å^2
6.2% VFF Fe Clusters in $Cu_{0.87}Al_{0.13}$Alloy Matrix	$r_1 = 2.56 \pm 0.01$ Å	$r_2 = 3.62 \pm 0.02$ Å	$r_3 = 4.49 \pm 0.02$ Å	$r_4 = 5.16 \pm 0.02$ Å
	$2\sigma_1^2 = 0.022 \pm 0.001$ Å^2	$2\sigma_2^2 = 0.033 \pm 0.007$ Å^2	$2\sigma_3^2 = 0.035 \pm 0.003$ Å^2	$2\sigma_4^2 = 0.033 \pm 0.004$ Å^2
5.1% VFF Fe Clusters in $Cu_{0.82}Al_{0.18}$Alloy Matrix	$r_1 = 2.57 \pm 0.01$ Å	$r_2 = 3.64 \pm 0.03$ Å	$r_3 = 4.53 \pm 0.02$ Å	$r_4 = 5.18 \pm 0.03$ Å
	$2\sigma_1^2 = 0.027 \pm 0.001$ Å^2	$2\sigma_2^2 = 0.035 \pm 0.007$ Å^2	$2\sigma_3^2 = 0.042 \pm 0.005$ Å^2	$2\sigma_4^2 = 0.041 \pm 0.007$ Å^2

the embedded Fe nanoparticles was retained with increasing Au-content in the alloy matrix.

Fig. 4 shows the k^3-weighted Fe K edge EXAFS spectrum $k^3\chi$, and associated Fourier transform for Fe nanoparticles embedded in a pure Al matrix. It is evident that the amplitude of $k^3\chi$ is a factor of six times lower for the Al-embedded Fe nanoparticles, when compared to the data in Fig. 2(vi) for the conventional Fe film. A two shell fit was applied to this data, with one Fe-Al shell and one Fe-Fe shell. The fit parameters r_i and $2\sigma_i^2$ and N_i obtained from this are listed in Table 4. The fit values for N_i indicate that Fe atoms are predominantly coordinated by Al rather than Fe. The fact that Al is a relatively light scatterer, and the relatively large fit value obtained for $\sigma^2_{Fe\text{-}Al}$, is consistent with the low amplitude of the EXAFS. It is also clear from these results that there is a considerable degree of alloying between the Fe nanoparticles and Al matrix. The fit values obtained for r_i are consistent with the bcc FeAl alloy structure [36].

3.2. Magnetometry

Magnetisation curves were measured for the films of Fe nanoparticles in a $Cu_{1-x}Al_x$ alloy matrix for four different atomic fractions of Al, and in a pure Cu matrix, at 2 K temperature. The magnetisation curves for the films of Fe nanoparticles embedded in (i) pure Cu matrix, (ii) $Cu_{0,87}Al_{13}$ alloy matrix and (iii) $Cu_{0,69}Al_{31}$ alloy matrix are displayed in Fig. 5. The magnetic moment values per atom for each of the five nanocomposite films were obtained using saturation magnetisation curves. These are shown in Fig. 6.

It is known from a previous study [17] that the atomic magnetic moments per Fe atom in $Cu_{1-x}Au_x$-embedded Fe nanoparticle films clearly increase with increasing Au-content in the alloy matrix. Increasing Au-content leads to stretching in the structure of the fcc matrix, and this stretch also caused a stretch in the structure of the fcc Fe nanoparticles in the alloy matrix. The controlled change and stretching of the atomic structure in the fcc Fe nanoparticles led to an increasing atomic magnetic moment to a high moment ferromagnetic state, with values of atomic moment as high as $2.5 \pm 0.3\ \mu_B$/atom. This result is broadly parallel with a number of works, for fcc Fe thin films grown on an alloy substrate [24,25,37,38], where lattice expansion leads to a high moment ferromagnetic state.

In the work presented here, for the Fe nanoparticles in a pure Cu matrix, the Fe magnetic moment was found to be $0.7\ \mu_B$/atom, while the atomic structure of the Fe nanoparticles was found to be fcc. This agrees with a previous report [17], where the crystal structure in Cu-embedded Fe nanoparticles at dilute concentrations of Fe nanoparticles was found to be fcc, and where the atomic Fe moments were between 0.4 and $0.9\ \mu_B$/atom. In the present study, it can be noted that the atomic moment in the Fe nanoparticles initially increases rapidly as the Al-content in the $Cu_{1-x}Al_x$ matrix is increased (see Fig. 6). The atomic moment for Fe nanoparticles in a $Cu_{0.87}Al_{0.13}$ matrix is already close to the value for bulk bcc Fe. As discussed in the previous section, Fe nanoparticles with both fcc and bcc structures are present in the embedded Fe nanoparticles when the Al-content in the matrix is low. Fe

Table 2
Structural parameters r_i and $2\sigma_i^2$ (interatomic distances and Debye–Waller factors respectively) obtained from fits to the Fe K edge EXAFS spectra measured for films of Fe nanoparticles embedded in a $Cu_{1-x}Al_x$ matrix. Also included the interatomic distances and coordinations in fcc Fe and bulk bcc Fe.

	Shell 1	Shell 2	Shell 3	Shell 4	Shell 5
fcc Fe	$r_1 = 2.54$ Å	$r_2 = 3.59$ Å	$r_3 = 4.40$ Å	$r_4 = 5.08$ Å	
	$N_1 = 12$	$N_2 = 6$	$N_3 = 24$	$N_4 = 12$	
5.8% VFF Fe Clusters in Cu Matrix	$r_1 = 2.53 \pm 0.01$ Å	$r_2 = 3.58 \pm 0.02$ Å	$r_3 = 4.43 \pm 0.02$ Å	$r_4 = 5.08 \pm 0.01$ Å	
	$2\sigma_1^2 = 0.018 \pm 0.001$ Å^2	$2\sigma_2^2 = 0.033 \pm 0.006$ Å^2	$2\sigma_3^2 = 0.032 \pm 0.003$ Å^2	$2\sigma_4^2 = 0.029 \pm 0.002$ Å^2	
Bulk bcc Fe	$r_1 = 2.49$ Å	$r_2 = 2.87$ Å	$r_3 = 4.06$ Å	$r_4 = 4.76$ Å	$r_5 = 4.97$ Å
	$N_1 = 8$	$N_2 = 6$	$N_3 = 12$	$N_4 = 24$	$N_5 = 8$
Fe MBE film	$r_1 = 2.48 \pm 0.01$ Å	$r_2 = 2.84 \pm 0.02$ Å	$r_3 = 4.07 \pm 0.01$ Å	$r_4 = 4.76 \pm 0.02$ Å	$r_5 = 4.96 \pm 0.02$ Å
	$2\sigma_1^2 = 0.011 \pm 0.001$ Å^2	$2\sigma_2^2 = 0.015 \pm 0.001$ Å^2	$2\sigma_3^2 = 0.022 \pm 0.003$ Å^2	$2\sigma_4^2 = 0.019 \pm 0.002$ Å^2	$2\sigma_5^2 = 0.017 \pm 0.003$ Å^2
6.8% VFF Fe Clusters in $Cu_{0.92}Al_{0.08}$Alloy Matrix	$r_1 = 2.50 \pm 0.01$ Å	$r_2 = 2.87 \pm 0.02$ Å	$r_3 = 4.04 \pm 0.02$ Å	$r_4 = 4.81 \pm 0.03$ Å	$r_5 = 5.00 \pm 0.02$ Å
	$2\sigma_1^2 = 0.014 \pm 0.001$ Å^2	$2\sigma_2^2 = 0.050 \pm 0.007$ Å^2	$2\sigma_3^2 = 0.035 \pm 0.003$ Å^2	$2\sigma_4^2 = 0.043 \pm 0.008$ Å^2	$2\sigma_5^2 = 0.034 \pm 0.006$ Å^2
6.2% VFF Fe Clusters in $Cu_{0.87}Al_{0.13}$Alloy Matrix	$r_1 = 2.49 \pm 0.01$ Å	$r_2 = 2.84 \pm 0.01$ Å	$r_3 = 4.07 \pm 0.02$ Å	$r_4 = 4.79 \pm 0.03$ Å	$r_5 = 4.99 \pm 0.02$ Å
	$2\sigma_1^2 = 0.014 \pm 0.001$ Å^2	$2\sigma_2^2 = 0.039 \pm 0.004$ Å^2	$2\sigma_3^2 = 0.034 \pm 0.004$ Å^2	$2\sigma_4^2 = 0.037 \pm 0.006$ Å^2	$2\sigma_5^2 = 0.032 \pm 0.006$ Å^2
5.1% VFF Fe Clusters in $Cu_{0.82}Al_{0.18}$Alloy Matrix	$r_1 = 2.49 \pm 0.01$ Å	$r_2 = 2.81 \pm 0.02$ Å	$r_3 = 4.09 \pm 0.02$ Å	$r_4 = 4.79 \pm 0.03$ Å	$r_5 = 4.97 \pm 0.02$ Å
	$2\sigma_1^2 = 0.016 \pm 0.001$ Å^2	$2\sigma_2^2 = 0.032 \pm 0.003$ Å^2	$2\sigma_3^2 = 0.036 \pm 0.004$ Å^2	$2\sigma_4^2 = 0.037 \pm 0.007$ Å^2	$2\sigma_5^2 = 0.031 \pm 0.006$ Å^2
6.0% VFF Fe Clusters in $Cu_{0.69}Al_{0.31}$Alloy Matrix	$r_1 = 2.50 \pm 0.01$ Å	$r_2 = 2.84 \pm 0.02$ Å	$r_3 = 4.10 \pm 0.02$ Å	$r_4 = 4.81 \pm 0.03$ Å	$r_5 = 4.92 \pm 0.06$ Å
	$2\sigma_1^2 = 0.016 \pm 0.001$ Å^2	$2\sigma_2^2 = 0.027 \pm 0.003$ Å^2	$2\sigma_3^2 = 0.032 \pm 0.004$ Å^2	$2\sigma_4^2 = 0.020 \pm 0.002$ Å^2	$2\sigma_5^2 = 0.049 \pm 0.010$ Å^2

Table 3
Structural parameters r_i and $2\sigma_i^2$ (interatomic distances and Debye–Waller factors respectively) obtained from 50% bcc – 50% fcc fits to the Fe K edge EXAFS spectra, measured for films of Fe nanoparticles embedded in a $Cu_{1-x}Al_x$ matrix. Also included are the coordinations N_i used in the fit.

	Film of Fe nanoparticles in $Cu_{0.92}Al_{0.08}$ alloy matrix	Film of Fe nanoparticles in $Cu_{0.87}Al_{0.13}$ alloy matrix
Shell 1a (bcc)	$r_{1a} = 2.49 \pm 0.01$ Å $2\sigma^2_{1a} = 0.011 \pm 0.001$ Å^2 $N_{1a} = 4$	$r_{1a} = 2.48 \pm 0.01$ Å $2\sigma^2_{1a} = 0.008 \pm 0.001$ Å^2 $N_{1a} = 4$
Shell 1b (fcc)	$r_{1b} = 2.55 \pm 0.01$ Å $2\sigma^2_{1b} = 0.024 \pm 0.003$ Å^2 $N_{1b} = 6$	$r_{1b} = 2.55 \pm 0.02$ Å $2\sigma^2_{1b} = 0.034 \pm 0.004$ Å^2 $N_{1b} = 6$
Shell 2a (bcc)	$R_{2a} = 2.86 \pm 0.01$ Å $2\sigma^2_{2a} = 0.027 \pm 0.003$ Å^2 $N_{2a} = 3$	$R_{2a} = 2.86 \pm 0.01$ Å $2\sigma^2_{2a} = 0.017 \pm 0.002$ Å^2 $N_{2a} = 3$
Shell 2b (fcc)	$R_{2b} = 3.56 \pm 0.02$ Å $2\sigma^2_{2b} = 0.025 \pm 0.004$ Å^2 $N_{2b} = 3$	$R_{2b} = 3.54 \pm 0.03$ Å $2\sigma^2_{2b} = 0.029 \pm 0.006$ Å^2 $N_{2b} = 3$
Shell 3a (bcc)	$R_{3a} = 4.08 \pm 0.01$ Å $2\sigma^2_{3a} = 0.021 \pm 0.002$ Å^2 $N_{3a} = 6$	$R_{3a} = 4.07 \pm 0.02$ Å $2\sigma^2_{3a} = 0.021 \pm 0.004$ Å^2 $N_{3a} = 6$
Shell 3b (fcc)	$R_{3b} = 4.37 \pm 0.02$ Å $2\sigma^2_{3b} = 0.043 \pm 0.006$ Å^2 $N_{3b} = 12$	$R_{3b} = 4.26 \pm 0.04$ Å $2\sigma^2_{3b} = 0.046 \pm 0.011$ Å^2 $N_{3b} = 12$
Shell 4a (bcc)	$R_{4a} = 4.82 \pm 0.01$ Å $2\sigma^2_{4a} = 0.022 \pm 0.002$ Å^2 $N_{4a} = 12$	$R_{4a} = 4.80 \pm 0.01$ Å $2\sigma^2_{4a} = 0.017 \pm 0.001$ Å^2 $N_{4a} = 12$
Shell 4b (fcc)	$R_{4b} = 5.29 \pm 0.02$ Å $2\sigma^2_{4b} = 0.022 \pm 0.004$ Å^2 $N_{4b} = 6$	$R_{4b} = 5.27 \pm 0.04$ Å $2\sigma^2_{4b} = 0.028 \pm 0.009$ Å^2 $N_{4b} = 6$

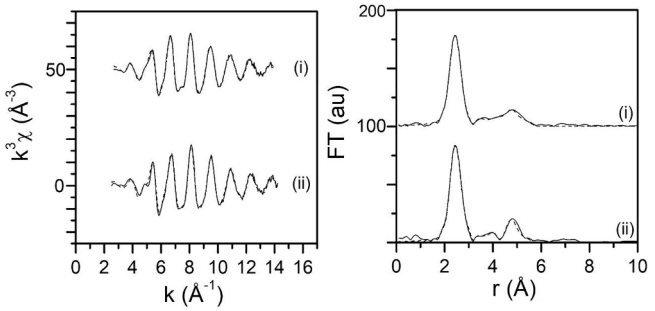

Fig. 3. Fe K edge EXAFS spectra χ, weighted by k^3, and associated Fourier transforms measured using two-shell fit for (i) a film of Fe nanoparticles embedded in $Cu_{0.92}Al_{0.08}$, (ii) a film of Fe nanoparticles embedded in $Cu_{0.87}Al_{0.13}$. The full line represents the data and Fourier transform of the data while the dashed line represents the fit to the data and Fourier transform of the fit.

nanoparticles embedded in an Ag matrix are known to have a bcc structure [15], and the same atomic moments as in bulk Fe [39]. The strong increase in atomic Fe moment with increasing Al-content seen

Table 4
Structural parameters r_i and $2\sigma_i^2$ (interatomic distances and Debye-Waller factors respectively) obtained from fits to the Fe K edge EXAFS spectrum measured for a film of Fe nanoparticles embedded in an Al matrix.

$r_{Fe\text{-}Al} = 2.52 \pm 0.02$ Å
$r_{Fe\text{-}Fe} = 2.55 \pm 0.03$ Å
$2\sigma^2_{Fe\text{-}Al} = 0.031 \pm 0.012$ Å^2
$2\sigma^2_{Fe\text{-}Fe} = 0.014 \pm 0.010$ Å^2
$N_{Fe\text{-}Al} = 6.5 \pm 0.9$
$N_{Fe\text{-}Fe} = 0.8 \pm 1.0$

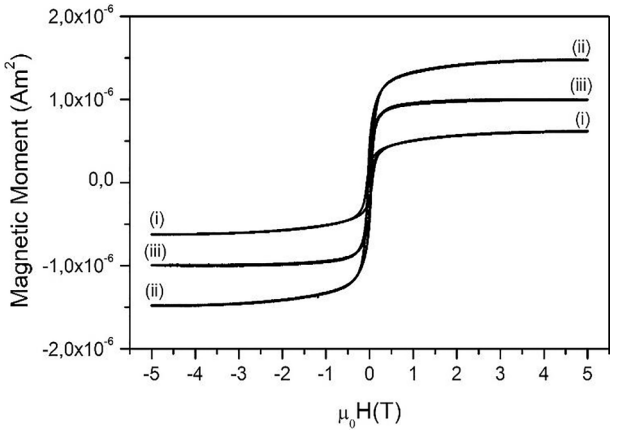

Fig. 5. Magnetization curves, showing total magnetic moment in the samples as a function of applied field, measured at 2 K for (i) a film of Fe nanoparticles in pure Cu, (ii) film of Fe nanoparticles in $Cu_{0,87}Al_{13}$ alloy matrix, (iii) film of Fe nanoparticles in $Cu_{0,69}Al_{31}$ alloy matrix. The equivalent thickness of Fe and the sample area for all samples was 350 Å and 25.5 mm^2 respectively.

here is therefore consistent with an increasing proportion of bcc Fe nanoparticles.

For Al-contents higher than 0.13, it can be seen that the net atomic moment value of Fe decreases slightly as the Al content in the $Cu_{1-x}Al_x$ alloy matrix is increased further. As discussed in detail in the structural analysis section, there is a high degree of alloying between Fe and Al atoms in a sample of Fe nanoparticles embedded in Al. Fig. 7 shows the magnetisation curve measured for this sample. The net atomic Fe moment, extracted from the saturation magnetisation, was found to be 0.39 μ_B/atom i.e. much lower than 2.2 μ_B/atom in bcc Fe. With increasing Al-content in the $Cu_{1-x}Al_x$ alloy matrix, a modest amount of alloying between Fe and Al atoms at the nanoparticle/matrix interface becomes more likely. This could explain the modest decrease observed in net atomic Fe moment at higher Al-content.

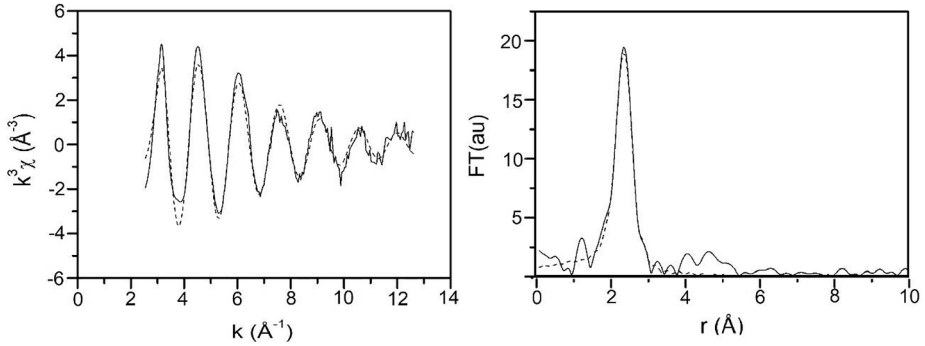

Fig. 4. Fe K edge EXAFS spectrum χ, weighted by k^3, and associated Fourier transform measured for a film of Fe nanoparticles embedded in Al with 5.9% VFF. The full line represents the data and Fourier transform of the data while the dashed line represents the fit to the data and Fourier transform of the fit.

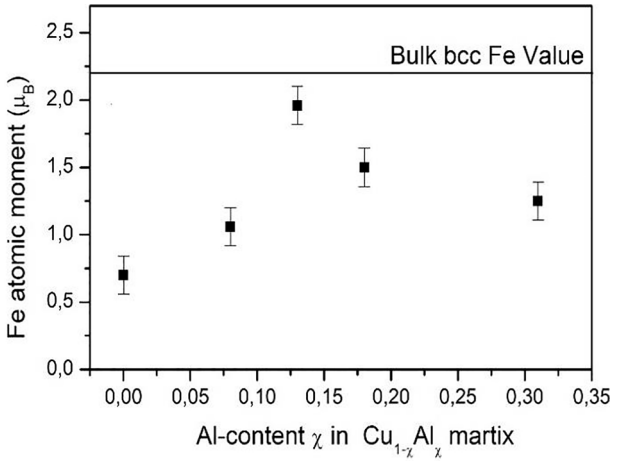

Fig. 6. Atomic moment in embedded Fe nanoparticles as a function of Al-content in the $Cu_{1-x}Al_x$ matrix.

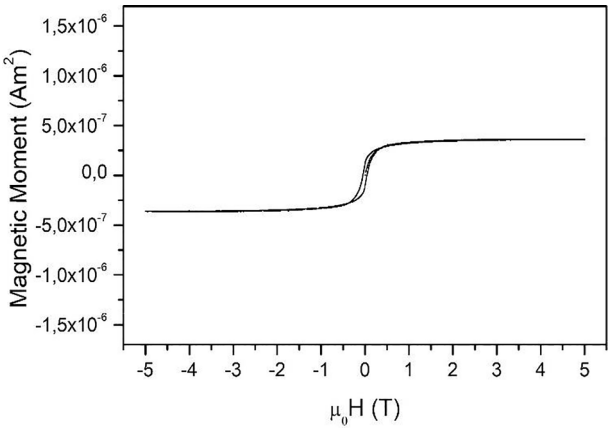

Fig. 7. Magnetization curve, showing total magnetic moment in the sample as a function of applied field for 5.9% VFF Fe in Al matrix at 2 K temperature.

4. Conclusions

We have measured the atomic structure and magnetism of Fe nanoparticles embedded in a $Cu_{1-x}Al_x$ matrix. EXAFS measurements show that Fe nanoparticles in $Cu_{0.82}Al_{0.18}$ and $Cu_{0.69}Al_{0.31}$ alloy matrices retain their bcc structure, while in $Cu_{0.92}Al_{0.08}$ and $Cu_{0.87}Al_{0.13}$ alloy matrices Fe nanoparticles have both fcc and bcc structures. The magnetic moment of Fe atoms for Fe nanoparticles in a $Cu_{1-x}Al_x$ matrix initially increases with increasing Al-content. This reflects the increased proportion of bcc Fe nanoparticles as the Al-content is increased. Beyond Al-contents of x = 0.13 the Fe atomic moment decreases, which is consistent with a modest degree of alloying between Fe and Al atoms at the nanoparticle/matrix interface.

Acknowledgment

The authors would like to thank Dr Stephen Parry for his invaluable advice and assistance during the EXAFS measurments at the Diamond Light Source.

References

[1] I.M.L. Billas, J.A. Becker, A. Châtelain, W.A. de Heer, Phys. Rev. Lett. 71 (1993) 4067.
[2] D.C. Douglass, A.J. Cox, J.P. Bucher, L.A. Bloomfield, Phys. Rev. B 47 (1993) 12874.
[3] D.C. Douglass, J.P. Bucher, L.A. Bloomfield, Phys. Rev. Lett. 68 (1992) 1774.
[4] S.H. Baker, C. Binns, K.W. Edmonds, M.J. Maher, S.C. Thornton, S. Louch, S.S. Dhesi, J. Magn. Magn. Mater. 247 (2002) 19.
[5] J.T. Lau, A. Fohlisch, R. Nietubye, M. Rief, W. Wurth, Phys. Rev. Lett. 89 (2002) 057201.
[6] J. Bansmann, S.H. Baker, C. Binns, J.A. Blackman, J.-P. Bucher, J. Dorantes-Dávila, V. Dupuis, L. Favre, D. Kechrakos, A. Kleibert, K.-H. Meiwes-Broer, G.M. Pastor, A. Perez, O. Toulemonde, K.N. Trohidou, J. Tuaillon, Y. Xie, Surf. Sci. Rep. 56 (2005) 189.
[7] A. Garćia Prieto, M.L. Fdez-Gubieda, A. Garćia-Arribas, J.M. Barandiaŕan, C. Meneghini, S. Mobilio, J. Magn. Magn. Mater. 221 (2000) 80.
[8] M.P.C. Vergara, J.C. Cezar, H.C.N. Tolentino, M. Knobel, Physica B 320 (2002) 143.
[9] J.C. Cezar, H.C.N. Tolentino, M. Knobel, Phys. Rev. B 68 (2003) 0544041.
[10] M. Jamet, V. Dupuis, P. Ḿelinon, G. Guiraud, A. Ṕerez, W. Wernsdorfer, A. Traverse, B. Baguenard, Phys. Rev. B 62 (2000) 493.
[11] J. Tuaillon, V. Dupuis, P. Ḿelinon, B. Ṕevel, M. Treilleux, A. Ṕerez, M. Pellarin, J.L. Vaille, M. Broyer, Phil. Mag. A 76 (1997) 493.
[12] V. Dupuis, M. Jamet, L. Favre, J. Tuiallon-Combes, P. Ḿelinon, A. Ṕerez, J. Vac. Sci. Technol. A 21 (2003) 1519.
[13] L. Favre, S. Stanescu, V. Dupuis, E. Bernstein, T. Epicier, P. Ḿelinon, A. Ṕerez, Appl. Surf. Sci. 226 (2004) 265.
[14] S.H. Baker, M. Roy, S. Louch, C. Binns, J. Phys.: Condens. Matter 18 (2006) 2385.
[15] S.H. Baker, M. Roy, S.J. Gurman, S. Louch, A. Bleloch, C. Binns, J. Phys.: Condens. Matter 16 (2004) 7813.
[16] M. Sakurai, S.A. Makhlouf, T. Hihara, K. Sumiyama, K. Wakoh, K. Suzuki, Physica B 208 (1995) 614.
[17] S.H. Baker, A.M. Asaduzzaman, M. Roy, S.J. Gurman, C. Binns, J.A. Blackman, Y. Xie, Phys. Rev. B 78 (2008) 014422.
[18] S.H. Baker, M. Roy, S.J. Gurman, C. Binns, J. Phys.: Condens. Matter 21 (2009) 183002.
[19] S.H. Baker, M. Roy, S.C. Thornton, C. Binns, J. Phys.: Condens. Matter 24 (2012) 176001.
[20] A. Perez, P. Melinon, V. Dupuis, P. Jensen, B. Prevel, J. Tuaillon, L. Bardotti, C. Martet, M. Treilleux, M. Broyer, M. Pellarin, J.L. Vialle, B. Palpant, J. Lerme, J. Phys. D: Appl. Phys. 30 (1997) 709.
[21] V.L. Moruzzi, P.M. Marcus, K. Schwarz, P. Mohn, Phys. Rev. B 34 (1986) 1784.
[22] D. Guenzburger, D.E. Ellis, Phys. Rev. B 51 (1995) 12519.
[23] V.L. Moruzzi, P.M. Marcus, J. Kübler, Phys. Rev. B 39 (1989) 6957.
[24] U. Gradmann, H.O. Isbert, J. Magn. Magn. Mater. 15–18 (1980) 1109.
[25] D.J. Keavney, D.F. Storm, J.W. Freeland, I.L. Grigorov, J.C. Walker, Phys. Rev. Lett. 74 (1995) 4531.
[26] V. Skumryev, S. Stoyanov, Y. Zhang, G. Hadjipanayis, D. Givord, J. Nogúes, Nature 423 (2003) 850.
[27] Q.A. Pankhurst, N.T.K. Thanh, S.K. Jones, J. Dobson, J. Phys. D: Appl. Phys. 42 (2009) 224001.
[28] B. Thiesen, A. Jordan, Int. J. Hyperth. 24 (2008) 467.
[29] S.H. Baker, S.C. Thornton, K.W. Edmonds, M.J. Maher, C. Norris, C. Binns, Rev. Sci. Instrum. 71 (2000) 3178.
[30] G.N. Iles, S.H. Baker, S.C. Thornton, C. Binns, J. Appl. Phys. 105 (2009) 024306.
[31] D. Stauffer, A. Aharony, Introduction to Percolation Theory, Taylor and Francis, 1994.
[32] A. Tenderholt, B. Hedman, K.O. Hodgson, 13th Int. Conf. XAFS, AIP Conf. Proc., 2007, p. 105.
[33] N. Binsted, EXCURV98: Daresbury, Laboratory Computer Program, 1998.
[34] S.J. Gurman, N. Binsted, I. Ross, J. Phys. C: Solid State Phys. 17 (1984) 143.
[35] M. Roy, S.J. Gurman, J. Synchrotron Radiat. 8 (2001) 1095.
[36] E.P. Yelsukov, E.V. Voronina, V.A. Barinov, J. Magn. Magn. Mater. 115 (1992) 271.
[37] W.A.A. Macedo, W. Keune, E.D. Ellerbrock, J. Magn. Magn. Mater. 93 (1991) 552.
[38] S. Mitani, A. Kida, M. Matsui, J. Magn. Magn. Mater. 126 (1993) 76.
[39] C. Binns, M.T. Qureshhi, D. Peddis, S.H. Baker, P.B. Howes, A. Boatwright, S.A. Cavill, S.S. Dhesi, L. Lari, R. Kröger, S. Langridge, Nano Lett. 13 (2013) 3334.